Oncogene (2015), 1–14

www.nature.com/onc

ORIGINAL ARTICLE

A novel pVHL-independent but NEMO-driven pathway in renal cancer promotes HIF stabilization

AM Nowicka[1], I Häuselmann[2], L Borsig[2], S Bolduan[3], M Schindler[3], P Schraml[1], M Heikenwalder[1,3,4,5] and H Moch[1,5]

Activation of hypoxia-inducible factor (HIF) is due to loss of von Hippel–Lindau protein (pVHL) function in most clear cell renal cell carcinomas (ccRCCs). Here we describe a novel pVHL-independent mechanism of HIF regulation and identify nuclear factor (NF)-κB essential modulator (NEMO) as a hitherto unknown oncogenic factor influencing human ccRCC progression. Over 60% of human ccRCCs ($n = 157$) have negative or weak NEMO protein expression by immunohistochemistry. Moderate/strong NEMO protein expression is more frequent in *VHL* wild-type ccRCCs. We show that NEMO stabilizes HIFα via direct interaction and independently of NF-κB signaling *in vitro*. NEMO prolongs tumor cell survival via regulation of apoptosis and activation of epithelial-to-mesenchymal transition, facilitating tumor metastasis. Our findings suggest that NEMO-driven HIF activation is involved in progression of ccRCC. Therefore, NEMO may represent a clinically relevant link between NF-κB and the VHL/HIF pathways. Targeting NEMO with specific inhibitors in patients with metastatic ccRCC could be a novel treatment approach in patients with ccRCC expressing functional pVHL.

Oncogene advance online publication, 26 October 2015; doi:10.1038/onc.2015.400

INTRODUCTION

The majority of clear cell renal cell carcinomas (ccRCCs) are characterized by loss of functional von Hippel–Lindau protein (pVHL) because of genetic mutation, deletion or hypermethylation of the *VHL* promoter.[1,2] pVHL triggers the oxygen-dependent proteasomal degradation of hypoxia-inducible factor α (HIFα), the main regulatory factor during hypoxia.[3,4] HIF1α and HIF2α are related transcription factors that regulate numerous genes directly connected to tumor development and progression.[5] Loss of pVHL function leads to HIFα stabilization and has been shown to be associated with tumor progression due to CXCR4 (chemokine (C-X-C motif) receptor 4) activation.[6] However, clinical studies failed to demonstrate any correlation between expression of HIFα or mutations in *VHL* and patient outcome in primary ccRCC.[7–9] Furthermore, pVHL loss was not sufficient to cause tumor formation.[10,11] Therefore, deregulation of the VHL/HIF axis alone may not be sufficient to induce metastasis. Recently, Vanharanta *et al.*[12] proposed that epigenetic modifications could modulate HIF target gene regulation and contribute to metastasis.

Renal cancer is resistant to radio- and chemotherapy.[13] The activation of nuclear factor-κB (NF-κB) transcription factor has been implicated in this poor response to therapy; however, the precise role of NF-κB signaling pathway in ccRCC has remained elusive.[14–16] NF-κB was also suggested to be a downstream target of pVHL loss and HIF activation,[17,18] but the interplay between HIF and NF-κB signaling has not been anticipated yet. The NF-κB essential modulator (NEMO) could represent the potential link between NF-κB and the VHL/HIF pathways. NEMO is a regulatory subunit of the IκB kinase (IKK) complex that functions to activate the NF-κB transcription factor through the canonical pathway.[19,20] NEMO regulates a number of cellular processes, including apoptosis and necrosis.[21–28] As an adaptor protein, NEMO was shown to stabilize its interaction partners as exemplified by interaction with ATM (ataxia telangiectasia mutated) during genotoxic stress or binding to c-Myc,[29–32] the activation of which was also demonstrated during renal tumor growth.[33–35] Previously, HIF2α was suggested as a binding partner of mouse Nemo in HEK293T cells.[36] Nevertheless, the role of NEMO in renal cancer was not elucidated so far. In this study we identify NEMO as the link between these two pathways and describe a novel alternative mechanism of HIF activation in ccRCC with functional pVHL.

RESULTS

NEMO expression is reduced in most human ccRCC tissue samples

To determine the prevalence of NEMO protein expression in renal cancer, we performed immunohistochemistry on tissue microarray (TMA) with different RCC subtypes.[37] The staining intensity obtained with a NEMO-specific antibody was assessed as negative, weak, moderate or strong, and was further quantified in an objective manner by densitometric, digital color-intensity analysis (Supplementary Figure S1a). Over 60% of ccRCC samples ($n = 157/250$) had negative or weak NEMO expression levels (Figure 1a and Supplementary Table S1). Reduced NEMO expression was significantly more frequent in ccRCC than in papillary RCC and oncocytoma, both representing renal cortical tumors with wild-type VHL ($P < 0.001$; Supplementary Figure S1b). Furthermore, we determined mRNA expression of *NEMO* by using data from previously performed DNA microarray analysis of frozen

[1]Institute of Surgical Pathology, University Hospital Zurich, Zurich, Switzerland; [2]Institute of Physiology, Zurich Center for Integrative Human Physiology, University of Zurich, Zurich, Switzerland; [3]Institute of Virology, Technische Universität München/Helmholtz Zentrum München, Munich, Germany and [4]Division of Chronic Inflammation and Cancer, German Cancer Research Center (DKFZ) Heidelberg, Heidelberg, Germany. Correspondence: Professor M Heikenwalder, Institute of Virology, Technische Universität München/Helmholtz Zentrum München, Schneckenburgerstrasse 8, Munich D-81675, Germany or Professor H Moch, Institute of Surgical Pathology, University Hospital Zurich, Schmelzbergstrasse 12, Zurich CH-8091, Switzerland.
E-mail: heikenwaelder@helmholtz-muenchen.de or holger.moch@usz.ch
[5]These authors contributed equally to this work.
Received 7 March 2015; revised 22 July 2015; accepted 14 August 2015

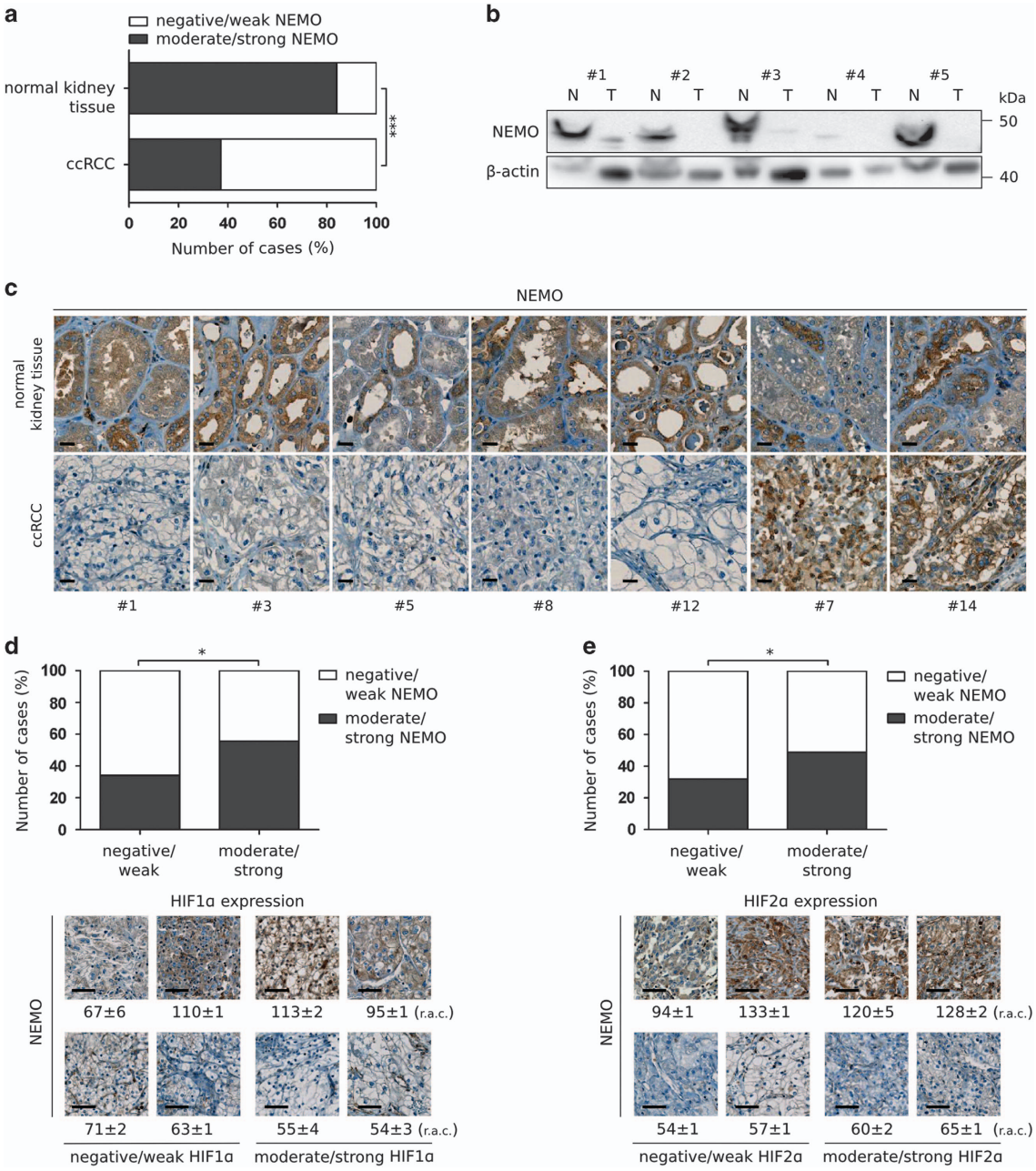

Figure 1. Expression of NEMO is decreased in ccRCC and correlates with HIF expression in ccRCC human tissue samples. (**a**) Immunohistochemical staining of NEMO on tissue microarray. Comparison of ccRCC and normal kidney human tissue samples; Pearson's χ^2 association test: $^{***}P < 0.001$. (**b**) Immunoblot analysis of indicated proteins in lysates from normal kidney (N) and corresponding ccRCC tumor (T) human tissue samples. (**c**) Immunohistochemical staining of NEMO on tissue microarray containing matched ccRCC and corresponding normal kidney human tissue samples. Scale bar: 20 μm. (**d**, **e**) Correlation between NEMO and HIF1α expression (**d**) or HIF2α expression (**e**) in ccRCC human tissue samples on tissue microarray and representative pictures of ccRCC immunohistochemically analyzed cases including the measured level of the staining intensity; Pearson's χ^2 association test: $^{*}P < 0.05$. Scale bar: 50 μm; r.a.c., relative area cover.

ccRCC tissue ($n = 74$).[38] Overall, we observed no difference in mRNA expression levels between different renal tumor subtypes and non-neoplastic renal tissue (Supplementary Figure S1c).

To analyze tumoral NEMO expression in comparison with normal renal tissue expression, we performed immunoblotting analysis for matched pairs of normal kidney and tumor tissues from 10 ccRCC patients (Figure 1b and Supplementary Figure S1d). Of the 10 cases, 6 (60%) exhibited significantly lower tumoral NEMO protein expression compared with matching normal renal tissue. Again, there were no differences in *NEMO* mRNA abundance (Supplementary Figure S1e). To verify this finding, we performed an immunohistochemical NEMO protein expression analysis in 15 matching pairs of normal/tumor samples using formalin-fixed, paraffin-embedded tissues (Figure 1c and Supplementary Table S2). This analysis also revealed negative or weak tumoral NEMO staining compared with moderate or strong NEMO expression in normal renal tissues in 11 of 15 patients (73%).

In 70–90% of ccRCCs, HIF1α and/or HIF2α subunits are stabilized because of loss of functional pVHL.[1,2,39] Therefore, we correlated NEMO expression with nuclear HIFα staining, indicating activated protein using our previously obtained HIF1α and HIF2α expression

data.[37,40] The degree of NEMO protein expression positively correlated with nuclear HIF1α and HIF2α staining ($P < 0.05$; Figures 1d and e and Supplementary Figure S2), as well as with the expression of different HIF targets (Supplementary Table S3).

NEMO is upregulated in VHL wild-type tumors

NEMO protein levels were compared with the *VHL* mutation status, which was previously reported.[41] Surprisingly, we observed that ccRCCs with *VHL* gene mutations displayed negative/weak NEMO protein expression more frequently than those with wild-type *VHL* gene ($P < 0.05$; Figure 2a). This was also verified by immunohistochemistry for pVHL (Supplementary Figure S3a). pVHL-negative ccRCCs showed more frequently negative/weak NEMO protein expression than pVHL-expressing tumors ($P < 0.05$; Figure 2b). To further account for promoter methylation-dependent inactivation of pVHL, we studied NEMO expression in two different cohorts of ccRCC patients: (1) those carrying *VHL* mutation leading to loss of pVHL expression and (2) those with wild-type *VHL* and pVHL expression (Supplementary Figure S3b). The statistical analysis revealed an even stronger correlation between NEMO expression and *VHL* status, confirming preferential NEMO expression in tumors with functional pVHL ($P < 0.001$). No such differences were observed for mRNA expression (Supplementary Figure S3c).

Subsequently, we elucidated whether we can reproduce this observation in cell lines with different endogenous pVHL expression. We used cell line microarray with a panel of RCC cell

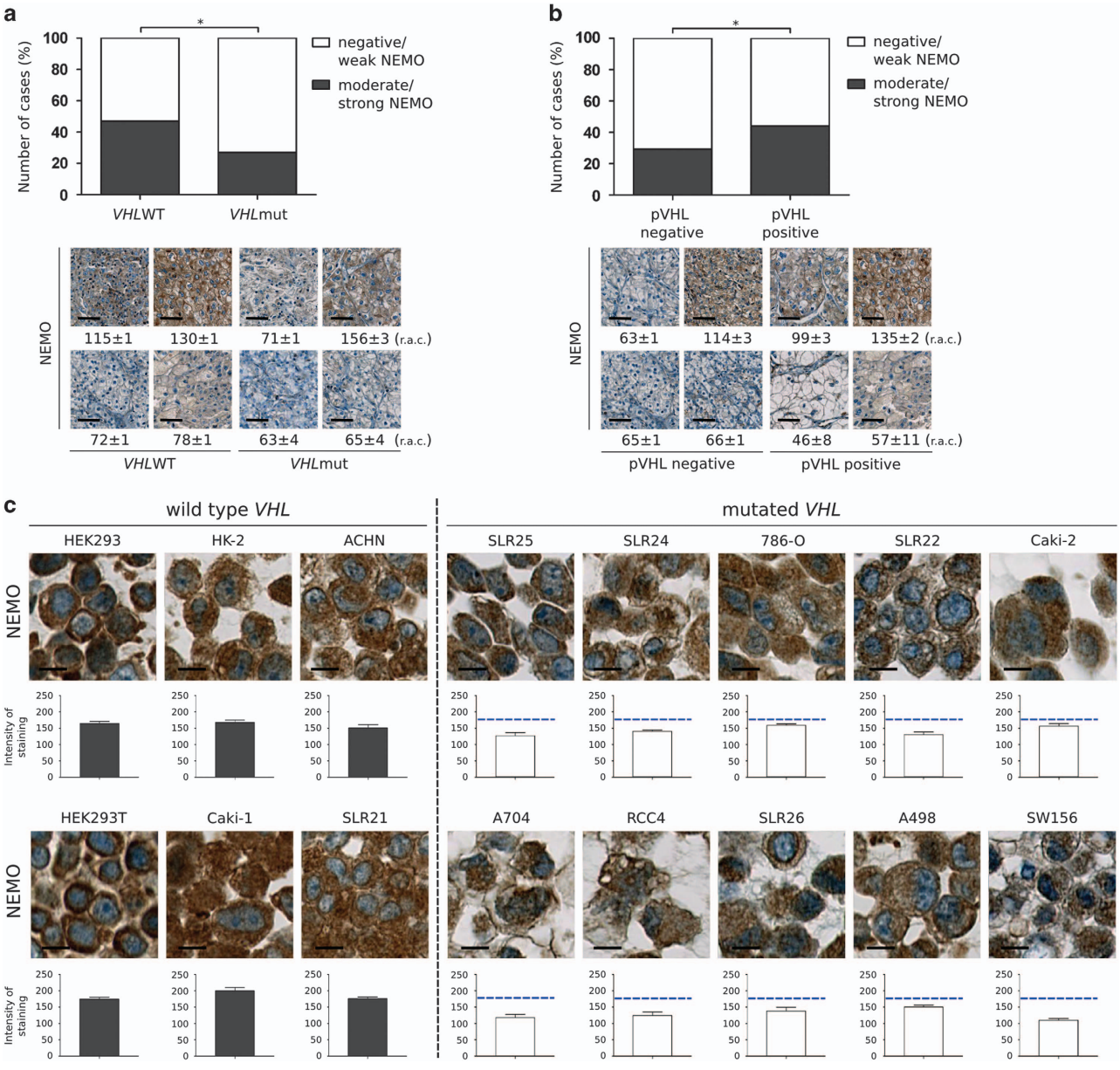

Figure 2. *VHL* wild-type tumors have increased NEMO expression. (**a**) Correlation of NEMO expression and *VHL* mutation status in ccRCC human tissue samples on tissue microarray and representative pictures of ccRCC immunohistochemically analyzed cases including the measured level of the staining intensity; Pearson's χ^2 association test: $^*P < 0.05$. Scale bar: 50 μm; r.a.c., relative area cover. (**b**) Correlation between NEMO and pVHL expression in ccRCC human tissue samples on tissue microarray and representative pictures of ccRCC immunohistochemically analyzed cases including the measured level of the staining intensity; Pearson's χ^2 association test: $^*P < 0.05$. Scale bar: 50 μm. (**c**) Immunohistochemical staining of NEMO on cell line microarray and quantification of the intensity of the staining from at least 20 random spots. Data are expressed as mean ± s.d. Scale bar: 10 μm.

lines exhibiting different *VHL* mutations, as well as normal proximal tubular HK-2 and kidney embryonic HEK293 cells.[42] Consistent with our human tissue data, NEMO expression was also higher in *VHL* wild-type cells ($P < 0.001$; Figure 2c and Supplementary Figure S3d). We next checked NEMO expression in RCC4 cells with introduced pVHL expression carrying type 2A and 2B missense mutations at positions Tyr98 and Tyr112 (Supplementary Figures S3e–h). NEMO expression was significantly decreased in cell lines with destabilized pVHL ($P < 0.001$). These findings show that NEMO is stronger expressed in ccRCCs

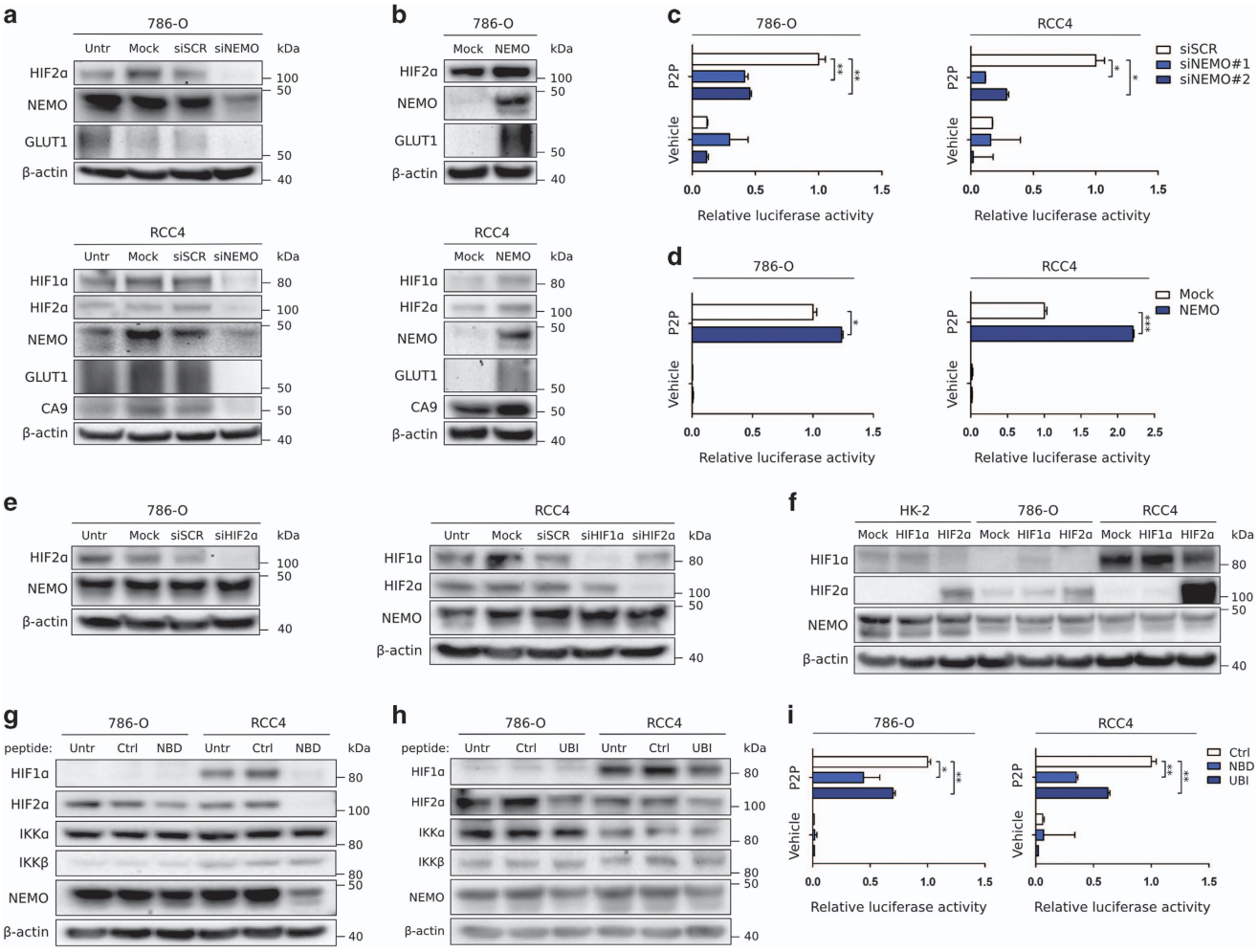

Figure 3. NEMO regulates HIF activation. (**a**, **b**) Immunoblot analysis of indicated proteins in lysates from 786-O and RCC4 cell lines after treatment with small interfering RNA (siRNA) against *NEMO* (**a**) and transient overexpression of NEMO (**b**). (**c**, **d**) Luciferase gene reporter assay. Relative luciferase activity differences in HIF activity after treatment with siRNA against *NEMO* (**c**) and after transient overexpression of NEMO (**d**). *Renilla* luciferase expression was used for normalization. Data are expressed as mean ± s.d. from two independent repeats. Student's *t*-test: $*P < 0.05$; $**P < 0.01$; $***P < 0.001$. (**e**) Immunoblot analysis of indicated proteins in lysates from 786-O and RCC4 cell lines after treatment with siRNA against *HIF1a* and *HIF2a*. (**f**) Immunoblot analysis of indicated proteins in lysates from HK-2, 786-O and RCC4 cell lines after transient overexpression of HIF1α and HIF2α. (**g**, **h**) Immunoblot analysis of indicated proteins in lysates from 786-O and RCC4 cell lines after treatment with NBD (**g**) and UBI (**h**) peptide inhibitors. The peptide consisting protein transduction (PTD) sequence derived from antennapedia was used as a control. (**i**) Luciferase gene reporter assay. Relative luciferase activity differences in HIF activity after treatment with NBD and UBI peptide inhibitors. *Renilla* luciferase expression was used for normalization. Data are expressed as mean ± s.d. from two independent repeats. Student's *t*-test: $*P < 0.05$; $**P < 0.01$. Results are representative of at least three independent experiments unless stated otherwise.

Figure 4. NEMO regulates HIFα via a direct protein–protein interaction. (**a**) Immunoblot analysis of indicated proteins after co-immunoprecipitation with anti-HA or anti-FLAG antibodies. Hemagglutinin (HA)-HIF1α, HA-HIF2α or FLAG-NEMO proteins were overexpressed in 786-O and RCC4 cell lines. (**b**) Immunoblot analysis of indicated proteins after co-immunoprecipitation with HIF1α, HIF2α or NEMO of endogenously expressed proteins in 786-O and RCC4 cell lines. (**c**) FACS-based FRET analysis of HEK293T cells transfected with YFP–NEMO and CFP–HIF1α or CFP–HIF2α proteins. Cells transfected with YFP and CFP alone or YFP–CFP fusion were used as a negative and positive control. Data are expressed as mean ± s.d. (**d**) Confocal microscopy analysis of localization of YFP-NEMO (in green) and CFP-HIF1α or CFP-HIF2α (in red) fusion proteins in HEK293T cell line. Representative pictures are presented in XYZ planes and 3D opacity. Arrows indicate 5 μm. (**e**) Immunoblot analysis of indicated proteins in 786-O and RCC4 cell lines after treatment with small interfering RNA (siRNA) against *NEMO* and subsequently with MG-132 inhibitor for 20 h. (**f**) Immunoblot analysis of indicated proteins in 786-O and RCC4 cell lines after treatment with siRNA against *NEMO* and subsequently with cycloheximide (CHX) for 0, 2, 4 and 8 h. (**g**) Immunoblot analysis of indicated proteins in 786-O and RCC4 cell lines after transient overexpression of NEMO and subsequent treatment with CHX for 0, 2, 4 and 8 h. Results are representative of at least three independent experiments.

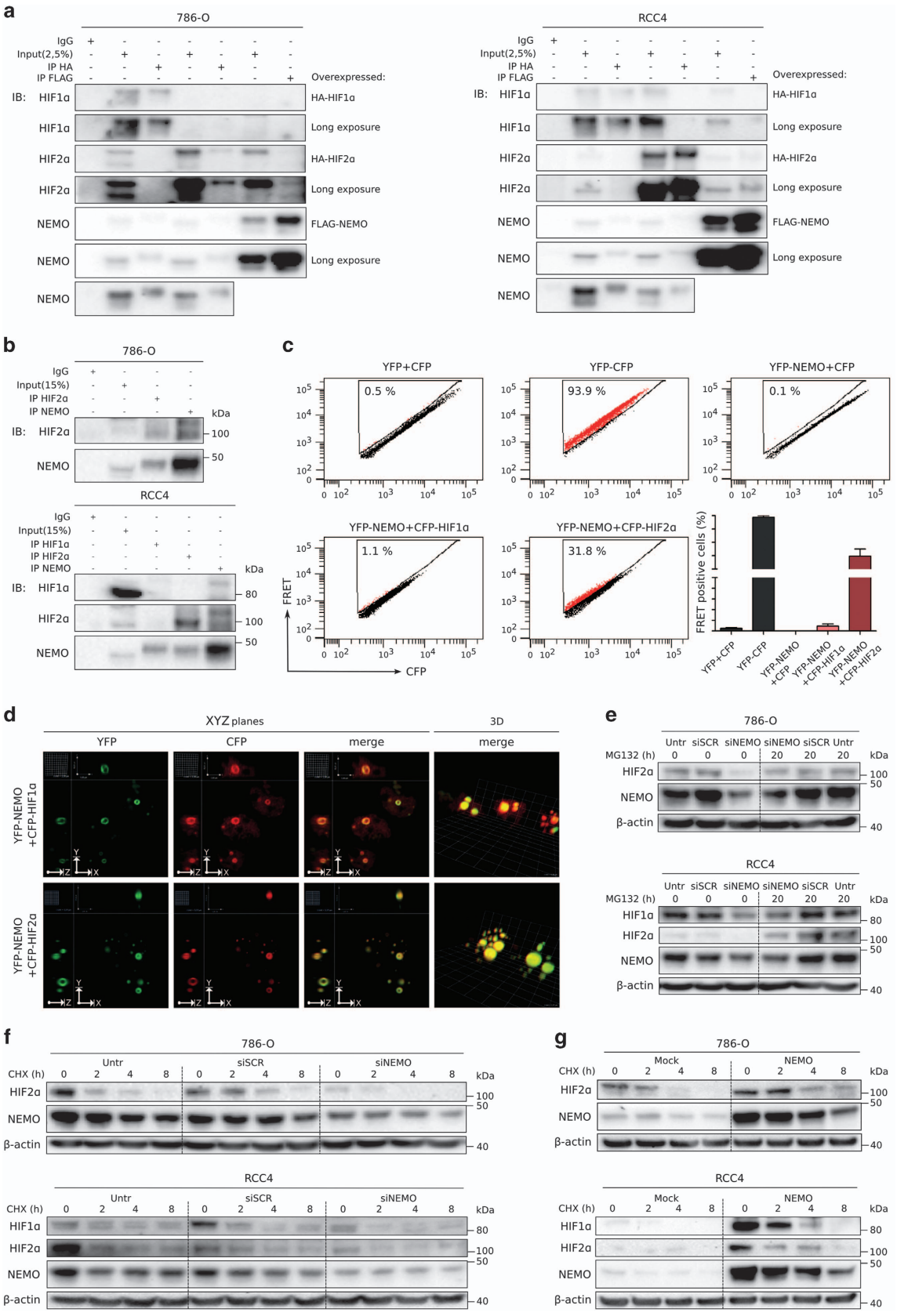

with wild-type *VHL*, although pVHL does not directly regulate NEMO expression.

HIFα subunits are downstream targets of NEMO

To further elucidate the exact role of NEMO in the regulation of the HIF signaling pathway, we performed *in vitro* experiments on ccRCC cell lines. *VHL* is mutated in most ccRCCs, therefore we used the 786-O and RCC4 cell lines lacking functional pVHL. 786-O cells constitutively express HIF2α, and RCC4 cells express both HIF1α and HIF2α (Supplementary Figure S4a). We silenced *NEMO* with two distinct small interfering RNA oligonucleotides that led to a decrease in protein expression of HIF1α and HIF2α (Figure 3a and Supplementary Figures S4b and c). Moderate silencing of NEMO (52 ± 18%) was already sufficient to cause a reproducibly strong HIFα downregulation (79 ± 11%). In contrast, transient overexpression of NEMO resulted in HIF1α and HIF2α upregulation (Figure 3b and Supplementary Figure S4d). The expression of the HIFα target genes *GLUT1* and *CA9* was similarly affected. It is noteworthy that *HIFα* subunit mRNA levels remained unchanged (Supplementary Figures S4e and f). NEMO silencing or overexpression also led to a transcriptional downregulation or activation of HIF, respectively, as measured by luciferase reporter assay (Figures 3c and d). Activation of κB-responsive elements was also affected, as seen by the luciferase reporter assay and by monitoring the expression of NF-κB target genes (Supplementary Figures S4g–j).

To determine the influence of HIFα on NEMO, we silenced both HIFα proteins in ccRCC cells (Figure 3e). The expression levels of NEMO remained unchanged. Furthermore, transient HIFα overexpression in 786-O, RCC4 and HK-2 cells did not affect NEMO expression (Figure 3f).

To confirm that NEMO activity functions as an upstream regulator of HIFα subunits, we used two NEMO peptide inhibitors: (1) NEMO binding domain inhibitor (NBD) that prevents IKK complex formation and (2) NEMO ubiquitin binding domain inhibitor (UBI) that specifically blocks NEMO activation by impeding ubiquitin binding to NEMO. Upon treatment with both inhibitors, protein expression of HIFα subunits in 786-O and RCC4 cells was decreased (Figures 3g and h), whereas mRNA levels remained unaffected (Supplementary Figure S5a). HIF and NF-κB transcription factors were also simultaneously downregulated (Figure 3i and Supplementary Figure S5b). Thus, NEMO positively regulates HIF1α and HIF2α protein expression.

NEMO stabilizes HIFα subunits

We investigated the mechanism of NEMO-HIFα regulation. As changes in HIFα expression occurred only on the protein level, and NEMO is a known scaffold protein, we hypothesized that NEMO stabilizes HIFα via direct binding. To test this hypothesis, we overexpressed FLAG-NEMO, hemagglutinin-tagged HIF1α or hemagglutinin-tagged HIF2α in 786-O and RCC4 cells and performed co-immunoprecipitation assay (Figure 4a). We observed binding between NEMO and HIF1α as well as HIF2α, with HIF2α being more efficiently pulled down. The same was observed for the endogenously expressed proteins (Figure 4b). In these experiments, immunoprecipitated proteins run slightly slower in comparison with that in protein extracts, presumably a result of the abundance of protein within immunoprecipitated samples and different salt content. In contrast, an interaction between NEMO and pVHL could not be detected (Supplementary Figure S6). We corroborated these findings using a flow cytometry-based Förster resonance energy transfer (FRET) assay.[43] It clearly indicated strong binding of NEMO to HIF2α and, in contrast, much weaker FRET of NEMO with HIF1α (Figure 4c). FRET efficiency can be optimized by increasing the

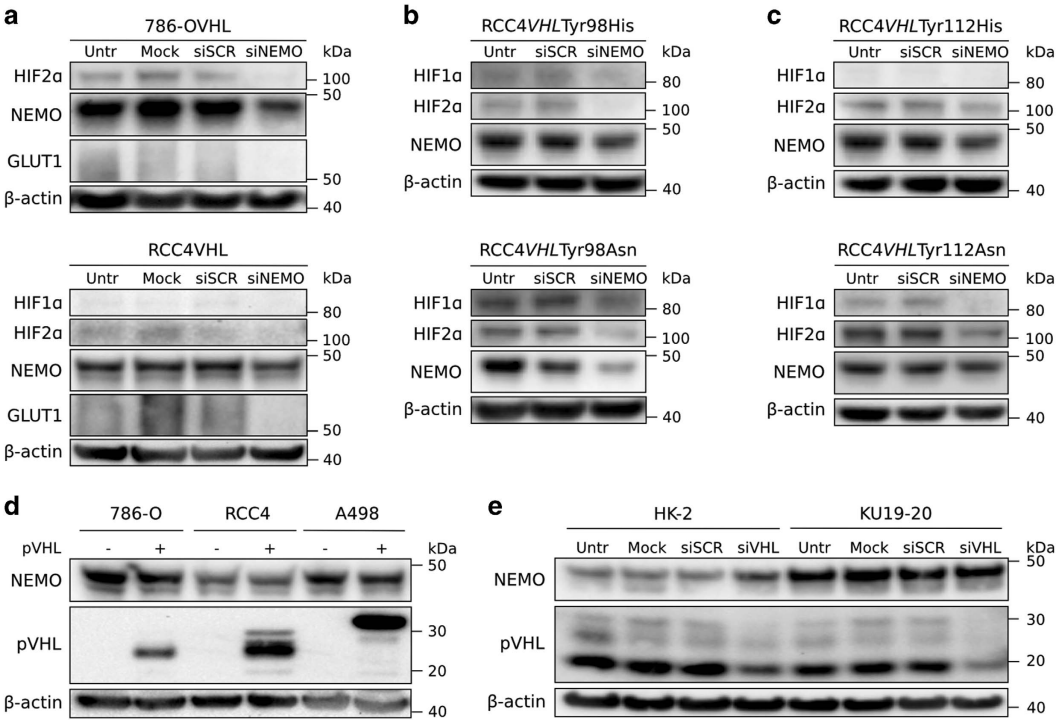

Figure 5. NEMO activates HIF signaling independently of pVHL. (**a**) Immunoblot analysis of indicated proteins in lysates from 786-O and RCC4 cell lines with reconstituted pVHL expression after treatment with small interfering RNA (siRNA) against *NEMO*. (**b**, **c**) Immunoblot analysis of indicated proteins in lysates from RCC4 cell line with reconstituted pVHL expression after treatment with siRNA against *NEMO*. *VHL* carries mutations at position Tyr98 (**b**) or Tyr112 (**c**) to His and Asn. (**d**) Immunoblot analysis of indicated proteins in lysates from 786-O, RCC4 and A498 cell lines not expressing or with reconstituted expression of pVHL. (**e**) Immunoblot analysis of indicated proteins in lysates from HK-2 and KU19-20 cell lines, endogenously expressing pVHL, after treatment with siRNA against *VHL*. Results are representative of at least three independent experiments.

amount of acceptor molecules to minimize unpaired donors. In line with this, we observed an increased FRET signal while increasing the ratio between yellow fluorescent protein (YFP)–NEMO and cyan fluorescent protein (CFP)–HIF1α or CFP–HIF2α expressing plasmids, also confirming the specificity of the weak binding between NEMO and HIF1α (Supplementary Figure S7a). Furthermore, both HIFα subunits colocalized with NEMO (Figure 4d and Supplementary Figure S7b).

We then investigated whether HIFα is stabilized upon binding to NEMO. Thus, we treated 786-O and RCC4 cells with the proteasome inhibitor MG-132, after previous silencing or inhibition of NEMO (Figure 4e and Supplementary Figures S8a and b). Blocking of proteasomal degradation restored the presence of HIFα, reversing the effect of small interfering RNA knockdown of NEMO. We also used cycloheximide to block protein synthesis. Silencing or inhibition of NEMO and treatment with cycloheximide resulted in faster destabilization and degradation of HIF1α and HIF2α (Figure 4f and Supplementary Figures S8c and d). On the other hand, HIF1α and HIF2α levels remained unaffected for a longer time in cells with overexpressed NEMO (Figure 4g). These data demonstrate that binding of NEMO protects HIFα subunits from proteasomal degradation and promotes its accumulation.

HIF activation is independent of pVHL presence

Subsequently, we checked whether NEMO-driven regulation of HIF1α and HIF2α depends on pVHL. We used 786-OVHL and RCC4VHL cell lines with reconstituted pVHL expression, leading to decreased levels of HIFα subunits (Supplementary Figure S4a). Silencing of NEMO in these cells caused a drop in the expression of HIF1α and HIF2α (Figure 5a). The NF-κB pathway was also affected, as indicated by the expression of target genes (Supplementary Figure S9a). Furthermore, we introduced point mutations at positions Tyr98 and Tyr112 into the *VHL* gene in RCC4VHL cells. Exchange of tyrosine for histidine is a type 2A

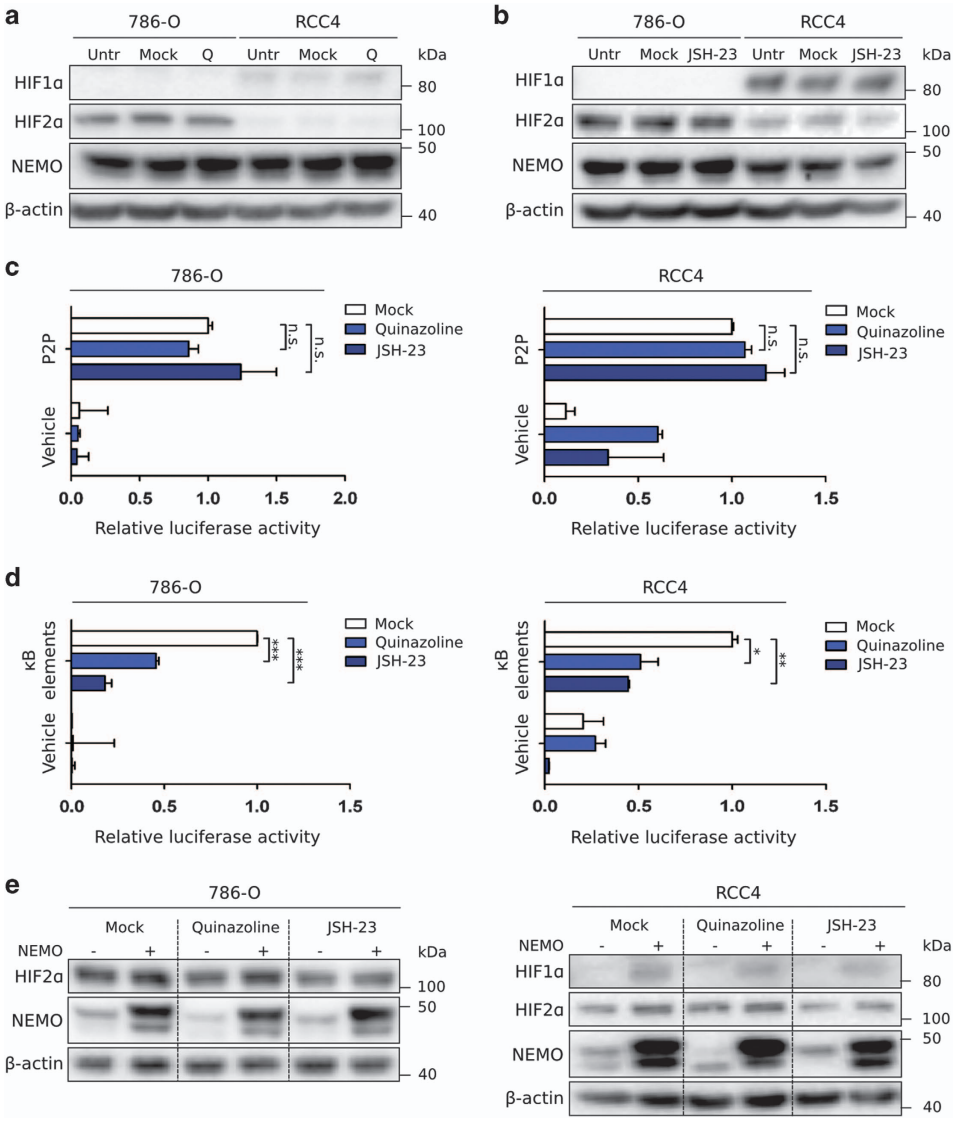

Figure 6. HIFα activation by NEMO is independent from NF-κB pathway. (**a**, **b**) Immunoblot analysis of indicated proteins in 786-O and RCC4 cell lines after treatment with 6-amino-4-(4-phenoxyphenylethylamino)quinazoline (Q) (**a**) and JSH-23 (**b**) inhibitors. (**c**, **d**) Luciferase gene reporter assay. Relative luciferase activity differences in HIF activity (**c**) and NF-κB activity (**d**) after treatment with 6-amino-4-(4-phenoxyphenylethylamino)quinazoline and JSH-23 inhibitors. *Renilla* luciferase expression was used for normalization. Data are expressed as mean ± s.d. from two independent repeats. Student's *t*-test: $*P < 0.05$; $**P < 0.01$; $***P < 0.001$; n.s., not significant. (**e**) Immunoblot analysis of indicated proteins in 786-O and RCC4 cell lines overexpressing NEMO and treated with NF-κB inhibitors. Results are representative of at least three independent experiments unless stated otherwise.

mutation and does not affect pVHL function with respect to HIFα degradation, whereas introduction of asparagine residues at these positions represents type 2B mutations leading to the destabilization of pVHL and HIFα accumulation. Silencing of NEMO resulted in decreased HIF1α and HIF2α expression levels, independently of pVHL stabilization (Figures 5b and c and Supplementary Figures S9b and c).

Next, we evaluated whether pVHL regulates the expression of NEMO. We used the pVHL-deficient ccRCC cell lines 786-O, RCC4 and A498 as well as their corresponding stable pVHL transfectants

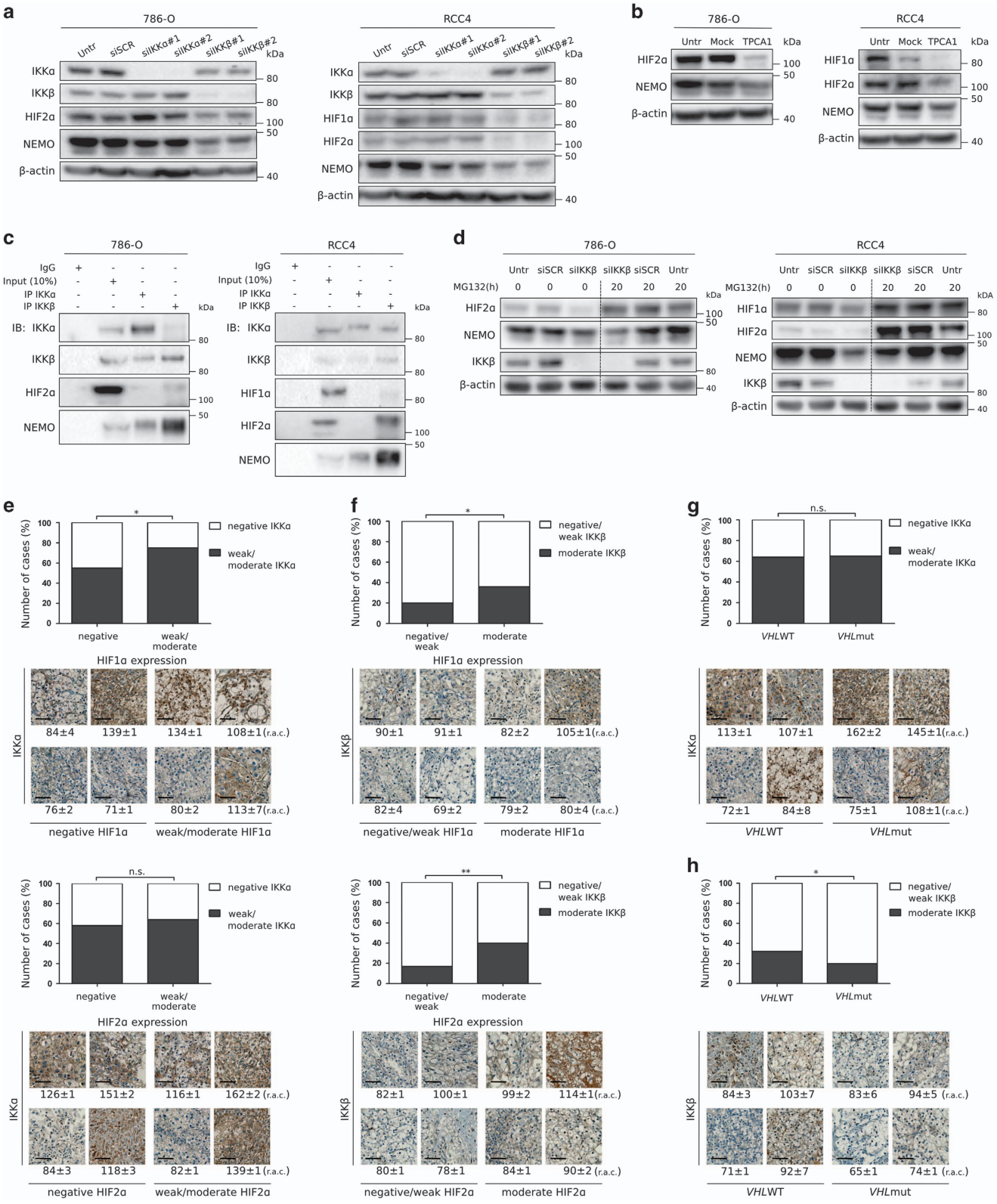

(Figure 5d and Supplementary Figure S9d). The levels of NEMO remained unchanged upon reintroduction of pVHL. Silencing of *VHL* in HK-2 and KU19-20 cell lines endogenously expressing pVHL also did not affect the expression of NEMO (Figure 5e and Supplementary Figure S9e). Altogether, our data demonstrated that pVHL does not directly regulate NEMO, and NEMO-mediated increase or decrease in HIFα subunit expression is independent of pVHL signaling.

NEMO regulates HIF independently of NF-κB signaling

NEMO is a member of the canonical NF-κB signaling cascade.[20] Therefore, we also tested the dependence of NEMO-HIFα regulation on the NF-κB transcription factor. We treated 786-O and RCC4 cells with the specific transcriptional inhibitors of p65 activation, 6-amino-4-(4-phenoxyphenylethylamino)quinazoline and JSH-23. The expression of HIF1α and HIF2α did not change in response to the treatment (Figures 6a and b and Supplementary Figure S10a). The transcriptional activation of HIF signaling also remained unaffected, although the κB-responsive elements were efficiently blocked, as shown by increased level of phosphorylated p65, reporter luciferase assay and expression of HIF and NF-κB target genes (Figures 6c and d and Supplementary Figures S10b–e). Subsequently, we used 786-O and RCC4 cells overexpressing NEMO and treated them with NF-κB transcriptional inhibitors (Figure 6e). This treatment did not abolish the effect of NEMO on HIFα subunit expression, confirming that NEMO induces HIF upregulation independently of NF-κB pathway.

IKKβ participates in HIFα stabilization

The IKK complex consists of two kinases IKKα and IKKβ and its regulatory subunit NEMO.[19] As the NBD peptide inhibitor disrupts the whole IKK complex, we examined whether the catalytic subunits of the IKK complex are necessary for HIF1α and HIF2α regulation. Knockdown of IKKβ, but not IKKα, resulted in a decrease of HIFα subunit expression (Figure 7a). Protein expression of NEMO was also reduced to a greater extent by IKKβ than by IKKα silencing. At the same time, activation of the NF-κB signaling pathway (κB-responsive elements) was strongly reduced upon IKKα as well as IKKβ silencing (Supplementary Figures S11a and b). To confirm the involvement of IKKβ in HIFα subunit stabilization, we treated cells with the IKKβ specific inhibitor TPCA1 that resulted in a drop of HIF1α and HIF2α levels (Figure 7b). Transcriptional activation of NF-κB was also blocked (Supplementary Figures S11c and d).

We next checked whether IKKβ forms a protein complex together with NEMO and HIF1α or HIF2α. Co-immunoprecipitation of IKKα and IKKβ confirmed that only IKKβ binds to both HIFα subunits (Figure 7c). To elucidate whether decreased level of IKKβ leads to HIF1α or HIF2α destabilization, we silenced or inhibited IKKβ followed by treatment with MG-132 inhibitor (Figure 7d and Supplementary Figure S11e). In both cases, HIF1α and HIF2α accumulated after incubation with MG-132. We also checked the expression levels of IKKβ upon silencing or overexpression of NEMO (Supplementary Figure S12a). No differences were observed, indicating a primary role of NEMO in HIFα stabilization. It is noteworthy that the expression of IKKβ was increased in the presence of pVHL in 786-O and RCC4 cells, suggesting that IKKβ might be needed for NEMO upregulation in the presence of wild-type *VHL* (Supplementary Figure S12b).

To elucidate the relevance of these data in human tissue *in situ*, RCC TMA was stained with antibodies for IKKα and IKKβ and subsequently quantified by measurement of staining intensity levels (Supplementary Figures S12c and d). Low expression of IKKα was associated with weak, nuclear staining of HIF1α ($P < 0.05$), but not HIF2α (Figure 7e). In contrast, expression of IKKβ significantly correlated with both HIF1α and HIF2α expression levels ($P < 0.05$ and $P < 0.01$ respectively; Figure 7f). As in the case of NEMO, the expression of IKKα and IKKβ also correlated with expression levels of different HIFα target genes (Supplementary Tables S4 and S5). Moreover, IKKα expression levels were independent of *VHL* mutation status, whereas the expression of IKKβ was increased when wild-type *VHL* was expressed ($P < 0.05$; Figures 7g and h).

NEMO promotes cell death and migration in ccRCC

We examined the impact of NEMO on cell viability and proliferation in 786-O and RCC4 cells. Treatment with NBD or UBI inhibitors exerted reduced metabolic activity as shown by the MTT assay (Figure 8a). We confirmed that observed cell death was caused by the activation of caspases leading to apoptosis and could be blocked by caspase inhibitor Q-VD-OPh (QVD) (Figure 8b and Supplementary Figure S13a). At the same time, the cell proliferation rate remained unchanged (Figure 8c). A similar observation was made upon silencing of NEMO with small interfering RNA (Figures 8d and e).

Subsequently, we analyzed whether inhibition of IKKβ activation also influences the cell death pathway. TPCA1 treatment caused a decrease in cell survival and induced caspase 3/7 activity (Figures 8f and g). In line, this effect was seen after silencing of *IKKβ* but not *IKKα* (Supplementary Figure S13b). It is noteworthy that cell proliferation was not affected by blocking IKKβ function (Figure 8h).

An important feature of cancer cells is their ability to migrate. We thus assessed the migration potential of the cells by performing a transmembrane migration assay of 786-O and RCC4 cells transiently overexpressing NEMO (Figure 8i). Cells with increased levels of NEMO migrated more efficiently through the membrane ($P < 0.001$ and $P < 0.05$ respectively). Epithelial-to-mesenchymal transition (EMT) is essential during tumor formation as well as in the later stages of tumor development.[44,45] Therefore, we checked whether the expression of several EMT markers changed upon overexpression of NEMO (Figure 8j). Many indicators of mesenchymal transition, like *Vimentin* or *SNAIL*, were significantly upregulated upon increased expression of NEMO. We also determined whether the increase of EMT markers is due to accumulation of HIFα subunits or activation of NF-κB signaling. Therefore, we used ccRCC cells stably overexpressing NEMO and silenced HIFα subunits or inhibited NF-κB (Supplementary Figures S14a and b). We observed that some genes like *CXCR7* are regulated through the HIF pathway, whereas others like *MMP9* are

Figure 7. IKKβ participates in HIFα stabilization. (**a**) Immunoblot analysis of indicated proteins in lysates from 786-O and RCC4 cell lines after treatment with small interfering RNAs (siRNAs) against *IKKα* and *IKKβ*. (**b**) Immunoblot analysis of indicated proteins in lysates from 786-O and RCC4 cell lines after treatment with TPCA1 inhibitor. (**c**) Immunoblot analysis of indicated proteins after co-immunoprecipitation with IKKα and IKKβ antibodies of endogenously expressed proteins in 786-O and RCC4 cell lines. (**d**) Immunoblot analysis of indicated proteins in 786-O and RCC4 cell lines after treatment with siRNA against *IKKβ* and subsequently with MG-132 inhibitor for 20 h. (**e**, **f**) Correlation between IKKα (**e**) or IKKβ (**f**) and HIF1α (upper panel) or HIF2α expression (lower panel) in ccRCC human tissue samples on tissue microarray and representative pictures of ccRCC immunohistochemically analyzed cases including the measured level of the staining intensity; Pearson's χ^2 association test: $^*P < 0.05$; $^{**}P < 0.01$; n.s., not significant; r.a.c., relative area cover. Scale bar: 50 μm. (**g**, **h**) Correlation between IKKα (**g**) or IKKβ (**h**) expression and *VHL* mutation status in ccRCC human tissue samples on tissue microarray and representative pictures of ccRCC immunohistochemically analyzed cases including the measured level of the staining intensity; Pearson's χ^2 association test: $^*P < 0.05$. Scale bar: 50 μm. Results are representative of at least three independent experiments.

regulated through NF-κB signaling. Levels of CXCR4 and c-Myc were shown to be elevated in metastatic ccRCC.[6,33,34,46,47] Therefore, we checked whether overexpression of NEMO can also cause activation of CXCR4 and c-Myc and demonstrated that expression levels of both proteins were increased when NEMO was overexpressed in ccRCC cells (Figures 8k and l and Supplementary Figure S15). These findings indicate that NEMO activates CXCR4 and c-Myc as well as regulates the expression of some EMT markers and therefore ccRCC progression.

NEMO is essential for ccRCC tumor progression

Our TMA analyses as well as *in vitro* data indicated a major role of NEMO in ccRCC formation. To further validate these observations

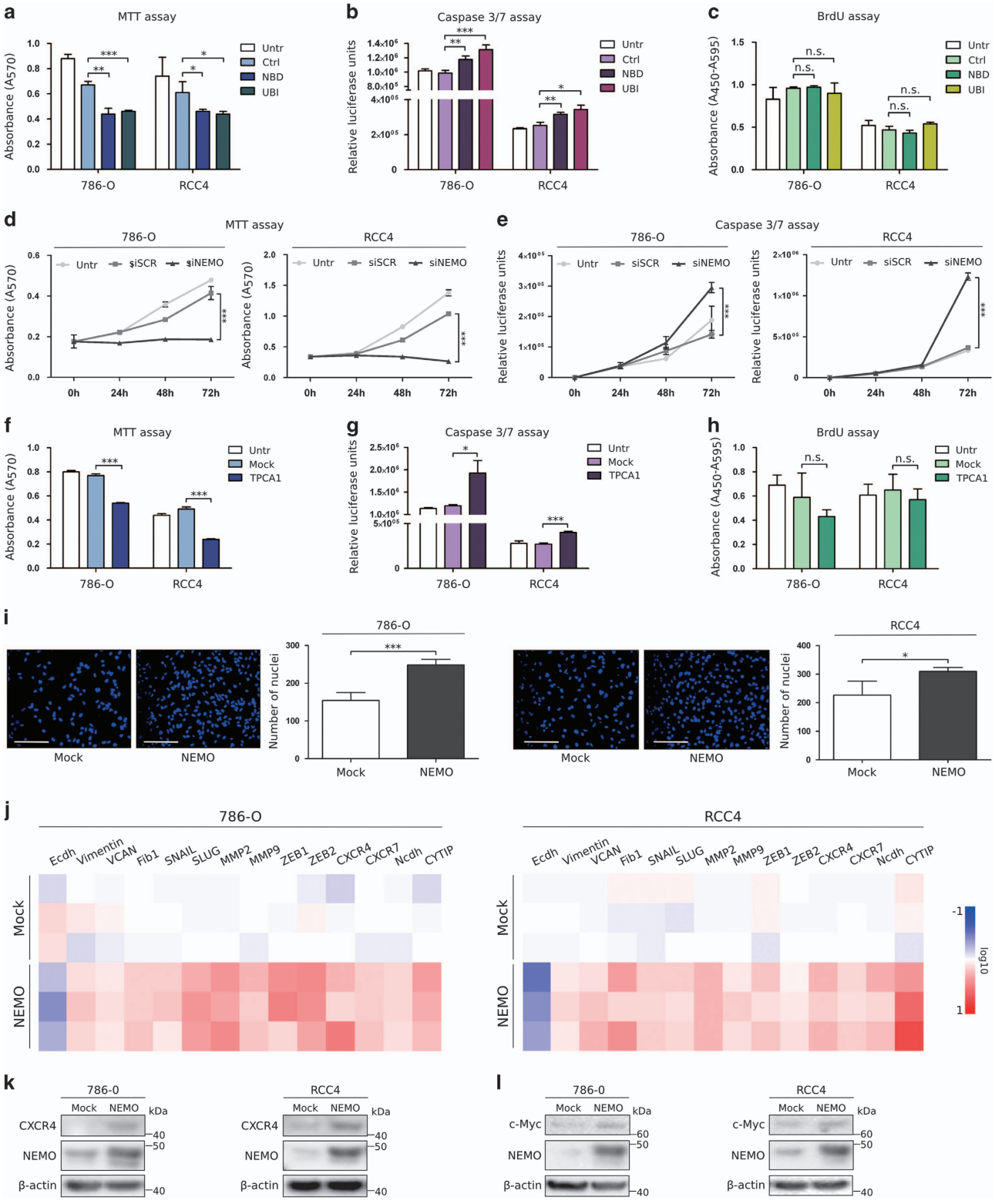

in situ, we correlated NEMO expression from our RCC TMA with available clinicopathological parameters of ccRCC patients (Supplementary Table S6). Moderate/strong NEMO protein expression was associated with poor histologic tumor differentiation grade ($P < 0.05$) and presence of sarcomatoid differentiation, associated with poor patient outcome ($P < 0.05$; Figure 9a and Supplementary Figures S16a and b). Although both parameters are strong biomarkers for poor patient outcome, there was no association with local tumor stage (pT category) at presentation and overall survival in patients with high NEMO expression (Supplementary Figures S16c and d).

In RCC, survival is mainly influenced by development of metastasis, and one of the most common metastatic sites of ccRCC is the brain.[48] To determine the relevance of NEMO in the process of metastasis, we used our recently described TMA with tissue samples from brain metastases of 52 ccRCC patients.[48,49] Strong NEMO staining was significantly more frequently observed in brain metastases ($n = 32/52$) than in primary tumors ($n = 93/250$; $P < 0.05$; Figure 9b), but no difference in the mRNA expression of *NEMO* was observed (Supplementary Figure S16e). Subsequently, we compared matched pairs of primary and metastatic ccRCC from 10 different patients (Figure 9c). In 7 of them (70%), there was higher NEMO expression in metastases than in matching primary tumors, suggesting that high NEMO expression facilitates brain metastasis.

To further determine the involvement of NEMO in metastasis, we used a lung metastasis mouse model. NOD/SCID (nonobese diabetic severe combined immunodeficient) mice were intravenously injected with RCC4 cells that express both HIF1α and HIF2α and stably overexpress NEMO. At 42 days after injection, mouse lungs were analyzed by histology (hematoxylin and eosin) and by immunohistochemistry with an antibody against GLUT1, a HIF target gene and marker for pVHL inactivation in ccRCC. GLUT1-positive tumor cells were detected in lung vessels of 60% of mice injected with cells overexpressing NEMO. In the case of controls with mock-transfected RCC4 cells, only one mouse (20%) showed GLUT1-positive tumor cells in the lungs ($P < 0.01$; Figure 9d). These data strongly indicate involvement of NEMO in metastasis of ccRCC.

DISCUSSION

In this study, we identified a novel mechanism of HIFα stabilization in ccRCC involving a member of the canonical NF-κB pathway. NEMO binds to HIFα subunits, thereby stabilizing HIFα and activating the HIF signaling pathway (Figure 9e). This NEMO-HIF regulation is independent of canonical NF-κB signaling and also occurs in the presence of pVHL—a negative regulator of HIFα. In addition, we showed that NEMO prevents cancer cells from entering apoptosis, promoting cancer cell survival and tumor metastasis.

The upregulation of HIF2α upon NEMO overexpression was previously indicated by Bracken *et al.*[36] By *in situ* and *in vitro* experiments we confirmed the role of NEMO as an upstream regulator of HIFα in ccRCC cells. HIF1α and HIF2α stabilization by NEMO leads to activation of HIF, as confirmed by luciferase gene reporter assay and expression levels of several HIF targets. To date, several research groups have reported NF-κB activation in ccRCC patients and have attempted to link it with tumor development.[15,50–52] Moreover, p62, an upstream regulator of NF-κB, was recently shown to promote renal carcinogenesis.[53] Our data demonstrate that NF-κB signaling *per se* does not directly participate in HIFα regulation, and previously observed activation of NF-κB could be a result of increased NEMO expression.

Furthermore, we identified a novel mechanism of NEMO-induced HIF activation. We showed that NEMO binds HIFα subunits and stabilizes them in ccRCC cells, leading to HIFα accumulation and transcriptional HIF activation. Nevertheless, interaction of NEMO with HIF1α appears to be weaker than with HIF2α and occurs less frequently. Previously, Sato *et al.*[2] identified another HIFα stabilization mechanism involving the *TCEB1* gene mutation (3% of ccRCC cases) that abrogates the interaction between pVHL and CUL2.

Importantly, especially ccRCCs with functional pVHL have elevated NEMO expression. Higher NEMO expression was also observed in papillary RCC and oncocytoma, both representing renal neoplasms without *VHL* mutations. Our *in vitro* experiments indicated that pVHL is not a direct regulator of NEMO. It is tempting to speculate that HIF1α and HIF2α stabilization by NEMO is particularly important for ccRCC with functional pVHL that constitutes 10 to 30% of all ccRCC, thus opening new therapeutic options.[1,39] Our findings may explain the HIF signaling pathway activation in the group of ccRCC patients with functional pVHL.

The IKK complex consists of two catalytic subunits IKKα and IKKβ.[54] Here, we show that silencing or inhibition of IKKβ, but not IKKα, results in downregulation of HIFα subunits and that IKKβ is present in the same complex with HIF1α or HIF2α. We also observed a drop in NEMO expression upon IKKβ silencing that, as a consequence, could affect HIFα stabilization. As IKKβ is a serine/threonine kinase, we hypothesize that IKKβ might phosphorylate NEMO during HIF regulation and activate it. Previously, it was reported that several posttranslational modifications lead to activation of NEMO. NEMO was shown to be phosphorylated by several kinases, including IKKβ.[55,56] Moreover, we observed elevated expression of IKKβ in the presence of wild-type *VHL*, and therefore activation of NEMO in ccRCC cases with functional pVHL could be a result of IKKβ upregulation. Although IKKβ plays a role in stabilization of HIFα, it does not seem to be essential for the whole process, as NEMO can activate the HIF pathway on its own.

Recently, we and others have shown that NEMO is important for development of liver, pancreatic and breast cancer.[21,26,27,57] We now present *in vivo* and *in vitro* data indicating that NEMO is also relevant for ccRCC progression. In addition, we show that NEMO prevents cancer cells from entering apoptosis and induces cell migration. We identified a tremendous increase in NEMO expression in human ccRCC metastases compared with their primary tumors. These data were corroborated using a mouse metastasis assay, demonstrating tumor thrombus formation in

Figure 8. NEMO induces apoptosis in ccRCC cells. MTT cell survival assay (**a**), caspase 3/7 apoptosis assay (**b**) and BrdU proliferation assay (**c**) in 786-O and RCC4 cell lines after treatment with NBD and UBI peptide inhibitors. Data are expressed as mean ± s.d. Student's *t*-test: $*P < 0.05$; $**P < 0.01$; $***P < 0.001$, n.s., not significant. MTT cell survival assay (**d**) and caspase 3/7 apoptosis assay (**e**) in 786-O and RCC4 cell lines after treatment with small interfering RNA (siRNA) against *NEMO* at different time points (0, 24, 48 and 72 h). Data are expressed as mean ± s.d. Student's *t*-test: $***P < 0.001$. MTT cell survival assay (**f**), caspase 3/7 apoptosis assay (**g**) and BrdU proliferation assay (**h**) in 786-O and RCC4 cell lines after treatment with TPCA1 inhibitors. Data are expressed as mean ± s.d. Student's *t*-test: $*P < 0.05$; $***P < 0.001$. (**i**) Representative pictures for transmembrane migration assay in 786-O and RCC4 cell lines transiently overexpressing NEMO. Nuclei were stained with DAPI and number of nuclei was quantified under the fluorescence microscope. Data are expressed as mean ± s.d. Student's *t*-test: $*P < 0.05$; $***P < 0.001$. Scale bar: 50 μm. (**j**) mRNA expression analysis (heat map) of EMT markers in 786-O and RCC4 cell lines after overexpression of NEMO. Data are presented as a mean of ΔΔCt values in log10 scale from three independent experiments (blue: downregulated, red: upregulated). (**k**, **l**) Immunoblot analysis of indicated proteins in lysates from 786-O and RCC4 cell lines after overexpression of NEMO. Results are representative of at least three independent experiments.

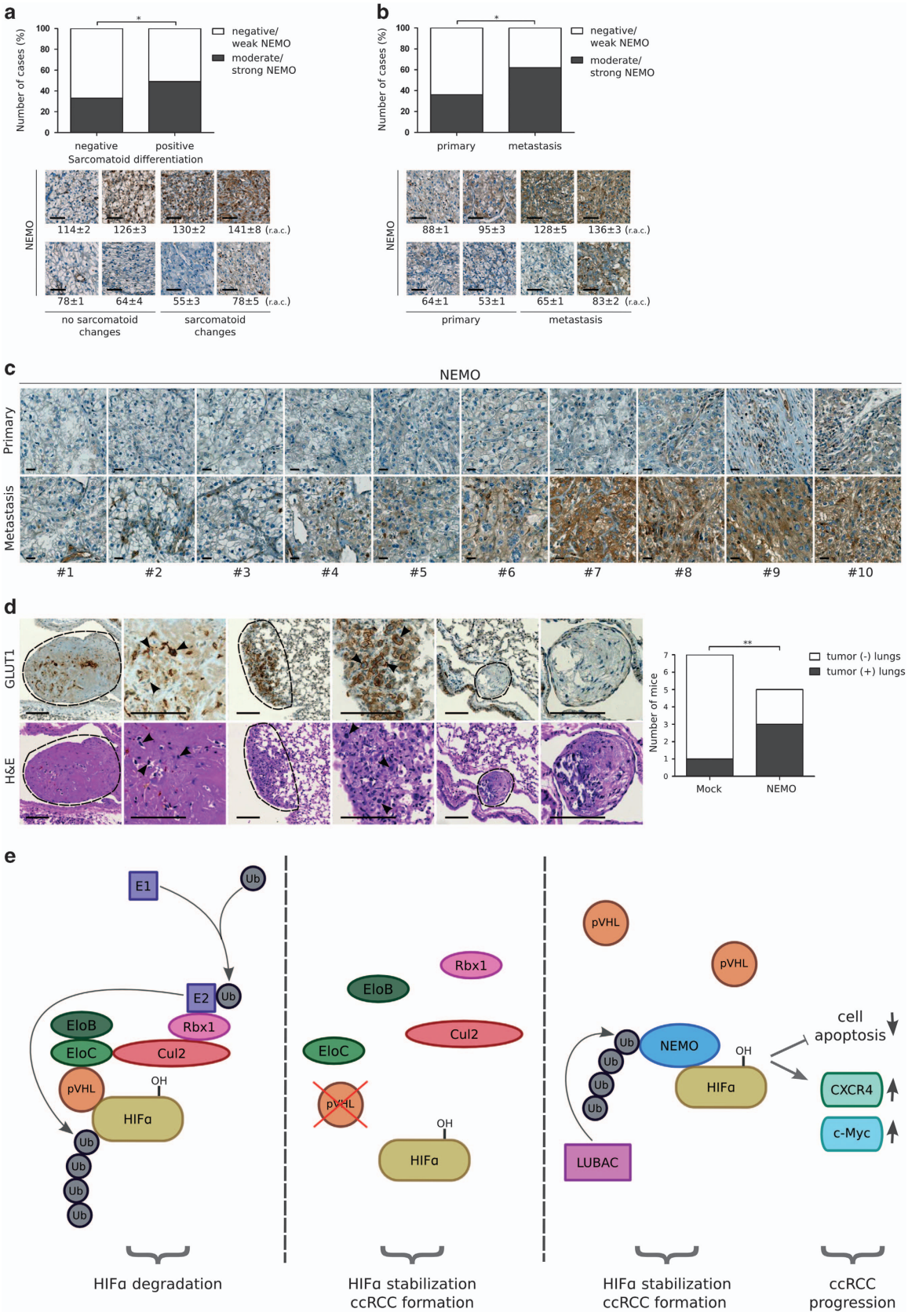

Figure 9. Elevated expression level of NEMO is associated with metastasis formation in ccRCC patients. (**a**) Correlation between NEMO expression and the presence of sarcomatoid differentiation in ccRCC human tissue samples on tissue microarray and representative pictures of ccRCC immunohistochemically analyzed cases including the measured level of the staining intensity; Pearson's χ^2 association test: $^*P < 0.05$. Scale bar: 50 μm; r.a.c., relative area cover. (**b**) NEMO expression in primary and metastatic ccRCC human tissue samples on tissue microarray and representative pictures of ccRCC immunohistochemically analyzed cases including the measured level of the staining intensity; Pearson's χ^2 association test: $^*P < 0.05$. Scale bar: 50 μm. (**c**) Immunohistochemical staining of NEMO on corresponding primary and metastatic human tissue samples from ccRCC patients. Scale bar: 20 μm. (**d**) Immunohistochemical hematoxylin and eosin (H&E) and GLUT1 staining on mouse lungs after intravenous (i.v.) injection of RCC4 cells stably overexpressing NEMO ($n = 5$) or mock transfected with an empty vector ($n = 7$) and quantification of mice with developed metastasis; Wilcoxon signed-ranks test: $^{**}P < 0.01$. Scale bar: 100 μm. (**e**) Model summarizing the proposed mechanism of HIFα subunit stabilization: In normoxia, pVHL recognizes hydroxylated HIF1α and HIF2α and targets them for polyubiquitin chain attachment followed by proteasomal degradation (left panel). In most of ccRCC tumors, pVHL is inactive and therefore HIFα subunits are stabilized, leading to tumor formation (middle panel). In normoxia, independently of pVHL presence, HIF1α and HIF2α is stabilized via interaction with NEMO, resulting in ccRCC tumor formation. NEMO activation also leads to the induction of cell survival and activation of CXCR4 and c-Myc followed by tumor metastasis (right panel).

lung vessels, with very few tumor cells invading surrounding tissues. This observation suggests that NEMO extends tumor cell survival, rather than increasing their invasive potential. As NEMO expression level was decreased in primary tumor compared with normal kidney tissue, NEMO signaling must be turned on in metastatic lesions at later tumor stages. Moreover, NEMO-induced HIF activation results in elevated expression of CXCR4 and c-Myc, factors with well-established roles in ccRCC progression. One-third of ccRCC patients exhibit locally advanced tumors and/or distant metastasis at the time of diagnosis and patients with metastatic ccRCC have poor prognosis.[7,13] Thus, targeting NEMO with specific inhibitors in patients with advanced disease could be a viable new approach to RCC therapy that might be particularly efficacious in patients with tumors expressing functional pVHL.

In summary, our results elucidate a novel function of NEMO in HIFα stabilization that is independent of canonical NF-κB signaling and pVHL presence. To date, HIF activation has been well defined in ccRCC biology as a driver of tumor formation.[3] Our data uncover an additional mechanism essential for ccRCC development, as well as reveal a novel signaling pathway leading to metastasis formation and therefore tumor progression. NEMO is ubiquitously expressed and has been demonstrated to be involved in different cancers. As hypoxia is a common feature of growing tumors, we hypothesize that the mechanism of HIF activation described here is a fundamental concept, not restricted to ccRCC.

MATERIALS AND METHODS

Tissue specimens and TMA construction

Four different TMAs comprising 262 ccRCC, 48 papillary, 15 chromophobe, 22 oncocytoma and 28 normal samples as well as 54 metastases with corresponding primary tissues (10 cases) or matched normal and primary ccRCC tissue samples (15 pairs) collected from the University Hospital Zurich (Zurich, Switzerland) were used. All tissue samples were histologically reviewed by one pathologist (HM) and selected on the basis of hematoxylin and eosin–stained tissue sections.[58] The composition of the TMAs and clinicopathological data has been previously described.[37,48,49] The cell line microarray composed of 23 different human cell lines originated from RCC or kidney was also used.[42] This study was approved by the Local Ethics Commission (reference number StV 38-2005).

Flow cytometry-based FRET assay

pECFP-N1 was used to generate N-terminal tagged fusions of CFP and HIF1α or HIF2α and pEYFP-C1 to generate N-terminal tagged fusions between YFP and NEMO. HEK293T cells were co-transfected with vectors expressing YFP–NEMO and CFP–HIF1α or CFP–HIF2α using the calcium phosphate method. FRET signals were measured by Flow cytometry 1 day post transfection using a FACS Cantoll (BD Bioscience, Heidelberg, Germany) according to the previously described protocol by Banning *et al.*[43] At least 2000 CFP/YFP-positive cells were analyzed for FRET.

Mice and lung colonization assay

Female, 7–8 weeks old NOD/SCID mice were purchased from Charles River Laboratories (Sulzfeld, Germany) and maintained under specific pathogen-free conditions. Experiments were approved by Zürich Cantonal Veterinary Committee according to the guidelines of the Swiss Animal Protection law. RCC4 cells (250 000) stably overexpressing NEMO or mock transfected were injected into lateral tail vein. Mice were killed after 6 weeks and lungs were harvested. In all, 5 mice were injected with RCC4 cells stably overexpressing NEMO and 7 mice with RCC4 mock-transfected cells (expressing an empty vector). Mouse lungs were blindly analyzed for the presence of tumor cells. No randomization method was used.

Statistical analysis

Statistical significance between experimental groups was assessed using an unpaired two-tailed Student's *t*-test (GraphPad Prism 5, La Jolla, CA, USA). Contingency table analysis and Pearson's χ^2 association tests for correlation assessment of TMA stainings, Wilcoxon signed ranks test for lung colonization assay analysis and univariate survival analysis by the Kaplan–Meier method and log-rank tests were used (IBM SPSS Statistics 21 software, Armonk, NY, USA). *P*-values of < 0.05 were considered statistically significant.

CONFLICT OF INTEREST

The authors declare no conflict of interest.

ACKNOWLEDGEMENTS

We thank M Bieri from University Hospital Zurich for preparing the script and establishing a novel formula for TMA staining intensity measurement, M Storz and S Dettwiler from the tissue biobank, A Fitsche, O Büchi and C Mittmann from the University Hospital Zurich for the excellent technical support, Professor I Frew from the University of Zurich and Dr T O'Connor from the Technical University of Munich for their critical input and reading the manuscript. This work was supported by the Swiss National Science Foundation Grants (3238BO-103145 and Sinergia) to HM; European Research Council (ERC) starting grant, a grant by the Stiftung für experimentelle Biomedizin (Peter-Hans Hofschneider foundation), the pre-clinical comprehensive center (PCCC), the SFB-TR36 and the Else Kröner-Fresenius Foundation to MH. AMN was supported by the NCCR-Kidney.ch.

REFERENCES

1 Cancer Genome Atlas Research Network, Comprehensive molecular characterization of clear cell renal cell carcinoma. *Nature* 2013; **499**: 43–49.
2 Sato Y, Yoshizato T, Shiraishi Y, Maekawa S, Okuno Y, Kamura T *et al.* Integrated molecular analysis of clear-cell renal cell carcinoma. *Nat Genet* 2013; **45**: 860–867.
3 Shen C, Kaelin Jr WG . The VHL/HIF axis in clear cell renal carcinoma. *Semin Cancer Biol* 2013; **23**: 18–25.
4 Frew IJ, Krek W. pVHL: a multipurpose adaptor protein. *Sci Signal* 2008; **1**: pe30.
5 Kaelin Jr WG, Ratcliffe PJ. Oxygen sensing by metazoans: the central role of the HIF hydroxylase pathway. *Mol Cell* 2008; **30**: 393–402.
6 Staller P, Sulitkova J, Lisztwan J, Moch H, Oakeley EJ, Krek W. Chemokine receptor CXCR4 downregulated by von Hippel-Lindau tumour suppressor pVHL. *Nature* 2003; **425**: 307–311.
7 Schlesinger-Raab A, Treiber U, Zaak D, Holzel D, Engel J. Metastatic renal cell carcinoma: results of a population-based study with 25 years follow-up. *Eur J Cancer* 2008; **44**: 2485–2495.

8 Schraml P, Struckmann K, Hatz F, Sonnet S, Kully C, Gasser T *et al.* VHL mutations and their correlation with tumour cell proliferation, microvessel density, and patient prognosis in clear cell renal cell carcinoma. *J Pathol* 2002; **196**: 186–193.
9 Young AC, Craven RA, Cohen D, Taylor C, Booth C, Harnden P *et al.* Analysis of VHL gene alterations and their relationship to clinical parameters in sporadic conventional renal cell carcinoma. *Clin Cancer Res* 2009; **15**: 7582–7592.
10 Frew IJ, Thoma CR, Georgiev S, Minola A, Hitz M, Montani M *et al.* pVHL and PTEN tumour suppressor proteins cooperatively suppress kidney cyst formation. *EMBO J* 2008; **27**: 1747–1757.
11 Rankin EB, Tomaszewski JE, Haase VH. Renal cyst development in mice with conditional inactivation of the von Hippel-Lindau tumor suppressor. *Cancer Res* 2006; **66**: 2576–2583.
12 Vanharanta S, Shu W, Brenet F, Hakimi AA, Heguy A, Viale A *et al.* Epigenetic expansion of VHL-HIF signal output drives multiorgan metastasis in renal cancer. *Nat Med* 2013; **19**: 50–56.
13 Fisher R, Gore M, Larkin J. Current and future systemic treatments for renal cell carcinoma. *Semin Cancer Biol* 2013; **23**: 38–45.
14 Morais C, Gobe G, Johnson DW, Healy H. Inhibition of nuclear factor kappa B transcription activity drives a synergistic effect of pyrrolidine dithiocarbamate and cisplatin for treatment of renal cell carcinoma. *Apoptosis* 2010; **15**: 412–425.
15 Oya M, Takayanagi A, Horiguchi A, Mizuno R, Ohtsubo M, Marumo K *et al.* Increased nuclear factor-kappa B activation is related to the tumor development of renal cell carcinoma. *Carcinogenesis* 2003; **24**: 377–384.
16 Sourbier C, Danilin S, Lindner V, Steger J, Rothhut S, Meyer N *et al.* Targeting the nuclear factor-kappaB rescue pathway has promising future in human renal cell carcinoma therapy. *Cancer Res* 2007; **67**: 11668–11676.
17 Yang H, Minamishima YA, Yan Q, Schlisio S, Ebert BL, Zhang X *et al.* pVHL acts as an adaptor to promote the inhibitory phosphorylation of the NF-kappaB agonist Card9 by CK2. *Mol Cell* 2007; **28**: 15–27.
18 An J, Rettig MB. Mechanism of von Hippel-Lindau protein-mediated suppression of nuclear factor kappa B activity. *Mol Cell Biol* 2005; **25**: 7546–7556.
19 Gilmore TD. Introduction to NF-kappaB: players, pathways, perspectives. *Oncogene* 2006; **25**: 6680–6684.
20 Rothwarf DM, Zandi E, Natoli G, Karin M. IKK-gamma is an essential regulatory subunit of the IkappaB kinase complex. *Nature* 1998; **395**: 297–300.
21 Bettermann K, Vucur M, Haybaeck J, Koppe C, Janssen J, Heymann F *et al.* TAK1 suppresses a NEMO-dependent but NF-kappaB-independent pathway to liver cancer. *Cancer Cell* 2010; **17**: 481–496.
22 Carvalho G, Fabre C, Braun T, Grosjean J, Ades L, Agou F *et al.* Inhibition of NEMO, the regulatory subunit of the IKK complex, induces apoptosis in high-risk myelodysplastic syndrome and acute myeloid leukemia. *Oncogene* 2007; **26**: 2299–2307.
23 Haybaeck J, Zeller N, Wolf MJ, Weber A, Wagner U, Kurrer MO *et al.* A lymphotoxin-driven pathway to hepatocellular carcinoma. *Cancer Cell* 2009; **16**: 295–308.
24 Irrinki KM, Mallilankaraman K, Thapa RJ, Chandramoorthy HC, Smith FJ, Jog NR *et al.* Requirement of FADD, NEMO, and BAX/BAK for aberrant mitochondrial function in tumor necrosis factor alpha-induced necrosis. *Mol Cell Biol* 2011; **31**: 3745–3758.
25 Legarda-Addison D, Hase H, O'Donnell MA, Ting AT. NEMO/IKKgamma regulates an early NF-kappaB-independent cell-death checkpoint during TNF signaling. *Cell Death Differ* 2009; **16**: 1279–1288.
26 Maier HJ, Wagner M, Schips TG, Salem HH, Baumann B, Wirth T. Requirement of NEMO/IKKgamma for effective expansion of KRAS-induced precancerous lesions in the pancreas. *Oncogene* 2013; **32**: 2690–2695.
27 Aigelsreiter A, Haybaeck J, Schauer S, Kiesslich T, Bettermann K, Griessbacher A *et al.* NEMO expression in human hepatocellular carcinoma and its association with clinical outcome. *Hum Pathol* 2012; **43**: 1012–1019.
28 Luedde T, Beraza N, Kotsikoris V, van Loo G, Nenci A, De Vos R *et al.* Deletion of NEMO/IKKgamma in liver parenchymal cells causes steatohepatitis and hepatocellular carcinoma. *Cancer Cell* 2007; **11**: 119–132.
29 Kim BY, Yang JS, Kwak SY, Zhang XK, Han YH. NEMO stabilizes c-Myc through direct interaction in the nucleus. *FEBS Lett* 2010; **584**: 4524–4530.
30 Sakamoto K, Hikiba Y, Nakagawa H, Hirata Y, Hayakawa Y, Kinoshita H *et al.* Promotion of DNA repair by nuclear IKKbeta phosphorylation of ATM in response to genotoxic stimuli. *Oncogene* 2013; **32**: 1854–1862.
31 Wu ZH, Shi Y, Tibbetts RS, Miyamoto S. Molecular linkage between the kinase ATM and NF-kappaB signaling in response to genotoxic stimuli. *Science* 2006; **311**: 1141–1146.
32 Yang Y, Xia F, Hermance N, Mabb A, Simonson S, Morrissey S *et al.* A cytosolic ATM/NEMO/RIP1 complex recruits TAK1 to mediate the NF-kappaB and p38 mitogen-activated protein kinase (MAPK)/MAPK-activated protein 2 responses to DNA damage. *Mol Cell Biol* 2011; **31**: 2774–2786.
33 Schultz L, Chaux A, Albadine R, Hicks J, Kim JJ, De Marzo AM *et al.* Immunoexpression status and prognostic value of mTOR and hypoxia-induced pathway members in primary and metastatic clear cell renal cell carcinomas. *Am J Surg Pathol* 2011; **35**: 1549–1556.
34 Tang SW, Chang WH, Su YC, Chen YC, Lai YH, Wu PT *et al.* MYC pathway is activated in clear cell renal cell carcinoma and essential for proliferation of clear cell renal cell carcinoma cells. *Cancer Lett* 2009; **273**: 35–43.
35 Gordan JD, Bertout JA, Hu CJ, Diehl JA, Simon MC. HIF-2alpha promotes hypoxic cell proliferation by enhancing c-myc transcriptional activity. *Cancer Cell* 2007; **11**: 335–347.
36 Bracken CP, Whitelaw ML, Peet DJ. Activity of hypoxia-inducible factor 2alpha is regulated by association with the NF-kappaB essential modulator. *J Biol Chem* 2005; **280**: 14240–14251.
37 Dahinden C, Ingold B, Wild P, Boysen G, Luu VD, Montani M *et al.* Mining tissue microarray data to uncover combinations of biomarker expression patterns that improve intermediate staging and grading of clear cell renal cell cancer. *Clin Cancer Res* 2010; **16**: 88–98.
38 Beleut M, Zimmermann P, Baudis M, Bruni N, Buhlmann P, Laule O *et al.* Integrative genome-wide expression profiling identifies three distinct molecular subgroups of renal cell carcinoma with different patient outcome. *BMC Cancer* 2012; **12**: 310.
39 Maher ER. Genomics and epigenomics of renal cell carcinoma. *Semin Cancer Biol* 2013; **23**: 10–17.
40 Luu VD, Boysen G, Struckmann K, Casagrande S, von Teichman A, Wild PJ *et al.* Loss of VHL and hypoxia provokes PAX2 up-regulation in clear cell renal cell carcinoma. *Clin Cancer Res* 2009; **15**: 3297–3304.
41 Rechsteiner MP, von Teichman A, Nowicka A, Sulser T, Schraml P, Moch H. VHL gene mutations and their effects on hypoxia inducible factor HIFalpha: identification of potential driver and passenger mutations. *Cancer Res* 2011; **71**: 5500–5511.
42 Pawlowski R, Muhl SM, Sulser T, Krek W, Moch H, Schraml P. Loss of PBRM1 expression is associated with renal cell carcinoma progression. *Int J Cancer* 2013; **132**: E11–E17.
43 Banning C, Votteler J, Hoffmann D, Koppensteiner H, Warmer M, Reimer R *et al.* A flow cytometry-based FRET assay to identify and analyse protein-protein interactions in living cells. *PLoS One* 2010; **5**: e9344.
44 Hanahan D, Weinberg RA. Hallmarks of cancer: the next generation. *Cell* 2011; **144**: 646–674.
45 Thiery JP, Acloque H, Huang RY, Nieto MA. Epithelial-mesenchymal transitions in development and disease. *Cell* 2009; **139**: 871–890.
46 Li G, Badin G, Zhao A, Gentil-Perret A, Tostain J, Peoc'h M *et al.* Prognostic value of CXCR4 expression in patients with clear cell renal cell carcinoma. *Histol Histopathol* 2013; **28**: 1217–1222.
47 Gassenmaier M, Chen D, Buchner A, Henkel L, Schiemann M, Mack B *et al.* CXC chemokine receptor 4 is essential for maintenance of renal cell carcinoma-initiating cells and predicts metastasis. *Stem Cells* 2013; **31**: 1467–1476.
48 Wyler L, Napoli CU, Ingold B, Sulser T, Heikenwalder M, Schraml P *et al.* Brain metastasis in renal cancer patients: metastatic pattern, tumour-associated macrophages and chemokine/chemoreceptor expression. *Br J Cancer* 2014; **110**: 686–694.
49 Vogetseder A, Thies S, Ingold B, Roth P, Weller M, Schraml P *et al.* alphav-Integrin isoform expression in primary human tumors and brain metastases. *Int J Cancer* 2013; **133**: 2362–2371.
50 Qi H, Ohh M. The von Hippel-Lindau tumor suppressor protein sensitizes renal cell carcinoma cells to tumor necrosis factor-induced cytotoxicity by suppressing the nuclear factor-kappaB-dependent antiapoptotic pathway. *Cancer Res* 2003; **63**: 7076–7080.
51 Konda R, Sugimura J, Sohma F, Katagiri T, Nakamura Y, Fujioka T. Over expression of hypoxia-inducible protein 2, hypoxia-inducible factor-1alpha and nuclear factor kappaB is putatively involved in acquired renal cyst formation and subsequent tumor transformation in patients with end stage renal failure. *J Urol* 2008; **180**: 481–485.
52 Meteoglu I, Erdogdu IH, Meydan N, Erkus M, Barutca S. NF-KappaB expression correlates with apoptosis and angiogenesis in clear cell renal cell carcinoma tissues. *J Exp Clin Cancer Res* 2008; **27**: 53.
53 Li L, Shen C, Nakamura E, Ando K, Signoretti S, Beroukhim R *et al.* SQSTM1 is a pathogenic target of 5q copy number gains in kidney cancer. *Cancer Cell* 2013; **24**: 738–750.
54 Hinz M, Scheidereit C. The IkappaB kinase complex in NF-kappaB regulation and beyond. *EMBO Rep* 2014; **15**: 46–61.
55 Palkowitsch L, Leidner J, Ghosh S, Marienfeld RB. Phosphorylation of serine 68 in the IkappaB kinase (IKK)-binding domain of NEMO interferes with the structure of the IKK complex and tumor necrosis factor-alpha-induced NF-kappaB activity. *J Biol Chem* 2008; **283**: 76–86.
56 Prajapati S, Gaynor RB. Regulation of Ikappa B kinase (IKK)gamma/NEMO function by IKKbeta -mediated phosphorylation. *J Biol Chem* 2002; **277**: 24331–24339.
57 Bist P, Leow SC, Phua QH, Shu S, Zhuang Q, Loh WT *et al.* Annexin-1 interacts with NEMO and RIP1 to constitutively activate IKK complex and NF-kappaB: implication in breast cancer metastasis. *Oncogene* 2011; **30**: 3174–3185.
58 Kononen J, Bubendorf L, Kallioniemi A, Barlund M, Schraml P, Leighton S *et al.* Tissue microarrays for high-throughput molecular profiling of tumor specimens. *Nat Med* 1998; **4**: 844–847.

Supplementary Information accompanies this paper on the Oncogene website (http://www.nature.com/onc)